Indium Tin Oxide Plasma Frequency Dependence on Sheet Resistance and Surface Adlayers Determined by Reflectance FTIR Spectroscopy

Scott H. Brewer and Stefan Franzen*

Department of Chemistry, North Carolina State University, Raleigh, North Carolina 27695

Received: July 24, 2002

Variable angle reflectance FTIR spectroscopy was used to investigate the optical properties of indium tin oxide (ITO) and fluorine-doped tin oxide (SFO) thin films in the near-IR spectral region. The reflectance data were used to determine the plasma frequency and the electronic scattering time using the Drude free-electron model, the dielectric function of ITO, and the two- and three-phase Fresnel equations for reflection. The reflectance, plasma frequency, and electronic scattering time of ITO thin films were found to be dependent on the sheet resistance. Surface adlayers were also found to affect the reflectance and the position of the plasma frequency of the ITO thin films. The reflectance and observed plasma frequency for the SFO thin films were lower than those for any of the ITO films studied.

Introduction

Indium tin oxide (ITO) thin films are widely used as infrared reflectors and transparent electrodes in the visible region of the electromagnetic spectrum.[1−11] These properties allow ITO thin films to be used in a wide range of optical and electronic applications such as heat shielding materials[12,13] and electrochemical sensors.[5,6] The optical properties of ITO thin films are highly sensitive to small variations in their preparation and annealing procedures.[12−16] Therefore, the preparation of these films to obtain desired optical properties is still an active area of research. Indium tin oxide thin films, similar to gold[17−24] and other metal oxides,[25,26] have been used as a substrate for modification with several different materials such as silanes,[27] amines,[28] carboxylic acids,[29,30] phosphonates,[30,31] thiols,[29,31] zirconium complexes,[3] tin complexes,[2] and DNA.[5] However, the effects of these adlayers on the properties of ITO depend on a firm understanding of the optical properties of the electrode material. Several different techniques have been used to investigate the properties of ITO such as spectroscopic ellipsometry,[32,33] X-ray photoelectron spectroscopy,[29] fixed angle reflection and transmission techniques,[7,13] diffuse reflectance FTIR spectroscopy,[34] and electrochemistry.[3,5,28,35,36] However, variable angle reflectance FTIR spectroscopy has not been fully utilized. This technique allows for the optical parameters of films with different preparations and annealing protocols to be determined in a nonintrusive manner in two sampling geometries. The reflectance and therefore optical properties of ITO can be determined from monitoring the reflectance with the light impinging directly on the ITO surface (air/ITO/glass substrate) or with the radiation first impinging on the glass substrate and then reflecting off the backside of the ITO surface (air/glass/ITO). These two sampling geometries offer flexibility in monitoring the affects on the optical properties of ITO thin films during annealing protocols or surface modification with adlayers (surface binding events).

The optical properties of ITO are a direct consequence of the position of the plasma frequency and the magnitude of the electronic scattering time as defined in the Drude free-electron model.[37,38] The plasma frequency for ITO occurs in the near-IR region, thus causing this material to be reflective in the mid-IR region and transparent in the visible region. Therefore, the position of the plasma frequency is critical in determining the optical properties of the material. In this study, the reflectance properties in the near-IR region were studied for ITO electrodes with varying sheet resistances. The Drude free-electron model was used to model the dielectric function of the ITO films to obtain values for the plasma frequency and electronic scattering times of the ITO thin films. The two- and three-phase Fresnel equations for reflection were then used to compare calculated and experimental reflectance infrared data. The reflectance of the ITO electrodes was studied with varying angles of incidence using p-polarized radiation. The effect of surface adlayers of 12-phosphonododecanoic acid and 1-hexadecanethiol on the optical properties (reflectivity and plasma frequency) of ITO thin films was also investigated. This surface adlayer effect is similar to surface plasmon resonance (SPR) that has typically been done on metal substrates;[39] however, this work proposes that SPR can also be done on metal oxide surfaces using reflectance FTIR spectroscopy in the near-IR region. Fluorine-doped tin oxide (SFO) thin films were also studied to aid in the understanding of how sheet resistance affects the optical properties of metal oxides, because this material is also a conducting metal oxide, but generally has a higher sheet resistance than ITO thin films.[40−42]

Materials and Methods

ITO and SFO Electrodes. Indium tin oxide (ITO) electrodes were obtained from Delta Technologies, Limited. The ITO electrodes were composed of 90% indium oxide and 10% tin oxide, had a nominal thickness of 1500 Å, and had a sheet resistance of 7−14 Ω/□. The substrate for the ITO electrodes was polished float (soda-lime) glass. The fluorine-doped tin oxide (SFO) thin films deposited on glass substrates were obtained from PPG Industries, Inc., and had a sheet resistance of ∼55 Ω/□, while the gold electrodes were obtained from Evaporated Metal Films, Inc. The ITO and SFO electrodes were cleaned for 20 min by UV/O_3 (UVO-cleaner (UVO-60), model

* To whom correspondence should be addressed. Phone: (919) 515-8915. Fax: (919) 515-8909. E-mail: Stefan_Franzen@ncsu.edu.

10.1021/jp026600x CCC: $22.00
Published on Web 11/22/2002

number 42, Jelight Company, Inc.) to yield a clean hydrophilic surface (as determined from contact angle measurements) (NRL C A. Goniometer (Rame-Hart, Inc.), model 100-00). The sheet resistances of these electrodes were measured with a 4-point probe consisting of a Signatone D27M probe station, a Keithley 224 programmable current source, and a Hewlett-Packard 3456A digital voltmeter.

Reflectance FTIR Spectroscopy. The variable angle reflectance FTIR spectra were recorded using a Spectra-Tech variable angle reflectance attachment (model 500) or the Bruker Auto-Seagull variable angle reflectance attachment in a Bruker IFS v/s spectrometer. The angle of incidence ranged from 40 to 80° relative to the surface normal. An infrared polarizer was used to obtain p-polarized light. A ratio of the single beam spectra of ITO or SFO electrodes to a single beam spectrum of a planar gold electrode was performed to obtain the reflectance spectra of ITO or SFO. A tungsten source, quartz beam splitter, and a liquid nitrogen cooled InSb detector were used in the spectral range 3000−13 000 cm^{-1}. All IR spectra were the result of the average of 512 scans at a resolution of 8 cm^{-1} and were recorded at room temperature under vacuum.

Theoretical Models

Drude Free-Electron Model. The Drude free-electron model describes the dielectric function ($\epsilon(\omega)$) of a material by the plasma frequency and electronic scattering time as shown in eq 1:[38]

$$\epsilon(\omega) = \epsilon_\infty - \omega_p^2 \frac{1}{\omega^2 + \frac{i\omega}{\tau}} \tag{1}$$

where ϵ_∞ is the high-frequency dielectric constant, ω_p is the plasma frequency, ω is the frequency, and τ is the electronic scattering time. The plasma frequency is defined in eq 2:[38]

$$\omega_p^2 = \frac{ne^2}{m\epsilon_o} \tag{2}$$

where n is the free charge carrier concentration, and m is the free-electron mass. Equation 3 relates the dielectric function to the complex refractive index of the material:[38]

$$\epsilon(\omega)^{1/2} = N(\omega) = n(\omega) + ik(\omega) \tag{3}$$

where N is the complex refractive index, n is the real, dispersive component, and k is the imaginary, absorptive component of the refractive index. This complex refractive index along with angle of incidence is used by the Fresnel equations of reflection for a two-phase (single dielectric interface) or three-phase system to model the reflectance of the material for p-polarized radiation.

Two-Phase Fresnel Equations for Reflectance. The two-phase Fresnel equations model the reflectance for a single dielectric interface. For instance, these equations model the air/ITO interface where the refractive index of ITO is complex (n and k components determined from the Drude free-electron model) and the refractive index of air (vacuum) is not complex (only a real component) and taken to be 1 ($n = 1$, $k = 0$). The ratios of the amplitudes of the reflected and incident light for p-polarized radiation for a single dielectric interface are shown in eqs 4 and 5:[37]

$$r_p = \frac{-N\cos\theta + \cos\varphi}{N\cos\theta + \cos\varphi} \tag{4}$$

where

$$\cos\varphi = \left(1 - \frac{\sin^2\theta}{N^2}\right)^{1/2} \tag{5}$$

In these equations, r is the amplitude of the reflected light (relative to incident light amplitude), p represents p-polarization, N is the complex refractive index of the material, θ is the angle of incidence relative to the surface normal, and ϕ is the complex angle between the refracted light to the surface normal. The power reflectivity for p-polarization is then shown in eq 6:[37]

$$R_p = |r_p|^2 \tag{6}$$

where R_p is the power reflectivity for p-polarization.

Three-Phase Fresnel Equations for Reflectance. The three-phase Fresnel equations of reflectance model a system composed of two dielectric interfaces. The system used in this analysis is air/ITO/glass, where the glass is the substrate on which the ITO thin film is deposited. The refractive index of air is again taken to only have a real component ($n = 1$, $k = 0$), and the complex dielectric function of ITO is determined from the Drude free-electron model, while literature values for the complex refractive index in the near-IR region for silicon dioxide (glass)[43] were used. The three-phase model takes into account the decay in the magnitude of the electric field through the ITO and the refraction of the light through this thin film before the radiation impinges on the ITO/glass interface. The general form of the ratio of the reflected and incident radiation for a three-phase model of the Fresnel equation is shown in eq 7:[44]

$$r_p = \frac{r_{p12} + r_{p23}e^{2i\beta}}{1 + r_{p12}r_{p23}e^{2i\beta}} \tag{7}$$

where r is the amplitude of reflected radiation, p refers to p-polarization, and the numerical subscripts (1, 2, 3) refer to the three phases (air, ITO, glass), respectively. β is defined in eq 8:[44]

$$\beta = 2\pi\left(\frac{h}{\lambda}\right)N_j\cos\Theta_j \tag{8}$$

where h is the thickness of layer j (taken to be 170 nm for ITO), λ is the wavelength of radiation, N is the complex index of refraction (eq 3) of layer j, and Θ is the angle relative to the surface normal in layer j. The general form of the two-phase Fresnel equations needed to determine r_{p12} and r_{p23} is defined in eq 9:[44]

$$r_{pjk} = \frac{N_j\cos\Theta_j - N_k\cos\Theta_k}{N_j\cos\Theta_j + N_k\cos\Theta_k} \tag{9}$$

where the subscripts j and k refer to the jth and kth phase of the model. Θ_k can be determined from eq 10:[44]

$$\cos\Theta_k = \left(1 - \frac{\sin^2\Theta_j}{N_k^2}\right)^{1/2} \tag{10}$$

where Θ_k is the angle in phase k relative to the surface normal. The power reflectivity or calculated reflectance, R_p, for p-polarized radiation is defined in eq 6.

Results and Discussion

Figure 1 shows the experimental variable angle reflectance FTIR spectra of a thin film of an indium tin oxide (ITO) on a

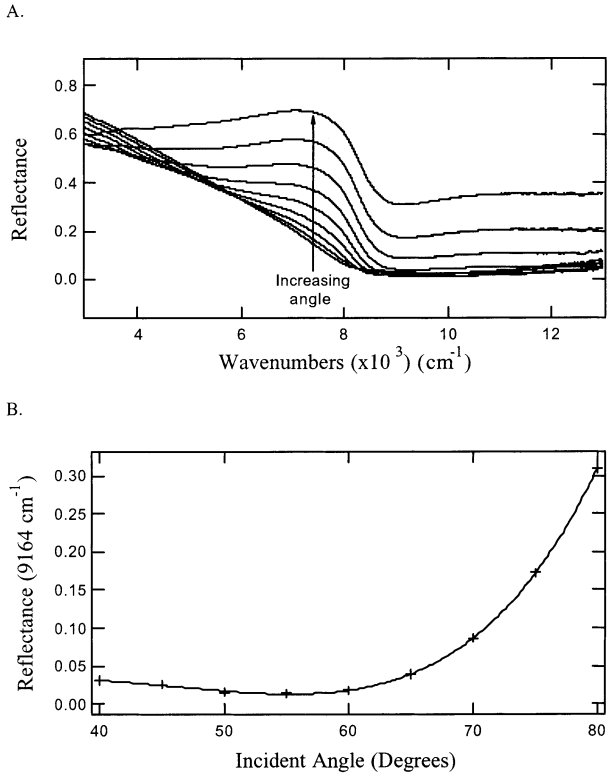

Figure 1. (A) Experimental variable angle reflectance FTIR spectra of a thin film of ITO (13.8 Ω/□) on a glass substrate relative to a gold surface in the near-IR region for incident angles ranging from 40 to 80° with p-polarized radiation (air/ITO sampling geometry). (B) Plot of the measured reflectance at 9164 cm^{-1} of ITO (13.8 Ω/□) as a function of incident angle for p-polarized radiation.

glass substrate in the near-IR region with a sheet resistance of 13.8 Ω/□. The measured reflectance was referenced to a gold surface. The angles of incidence were varied between 40 and 80 degrees relative to the surface normal using p-polarized IR radiation. Overall, the reflectance spectra of ITO show relatively high reflectance below ∼7500 cm^{-1}, and then the reflectance drops substantially. This sharp change in the reflectivity of the ITO is due to the plasma frequency (as defined in the Drude free-electron model) of the material. The plasma frequency is characterized by a sharp decrease in the measured reflectance of a material. Therefore, ITO is reflective below the plasma frequency and transparent at higher wavenumbers. However, the reflectance and transmittance of the material are dependent on the angle at which the radiation impinges on the material as shown in Figure 1. The observed value of the plasma frequency shifted to lower energy as the incident angle decreased. The position of the plasma frequency did not change with varying angles of incidence for s-polarized radiation as expected by the Fresnel equations for reflection (data not shown). Figure 1B shows the angle dependence of the reflection of an ITO thin film (13.8 Ω/□) for p-polarized radiation at 9164 cm^{-1}. This plot shows a minimum in the experimental reflectance of ITO, as expected from the Fresnel equations of reflection (data not shown), at ∼ 55°. These same trends in ITO reflectance and plasma frequency were found on ITO thin films deposited on fused quartz substrates (see Supporting Information).

Figure 2A,B,C shows a comparison of the experimental reflectance FTIR and calculated power reflectivity for p-polarized IR radiation of an ITO thin film deposited on a glass (soda-lime) substrate for incident angles of 40, 60, and 80° with a sheet resistance of 13.8 Ω/□. The power reflectivity of this

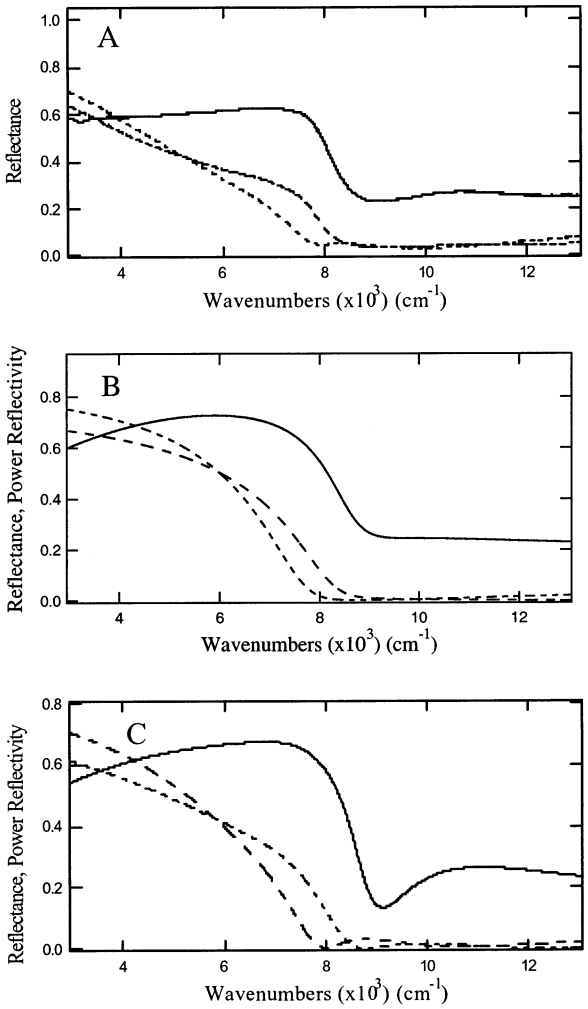

Figure 2. Experimental (A) and calculated (B, C) reflectance spectra for incident angles of 40 (short dashed), 60 (long dashed), and 80° (solid) for ITO on a glass substrate with a sheet resistance of 13.8 Ω/□ recorded or calculated with p-polarized radiation in the near-IR region. The calculated reflectance spectra of ITO used either the two-phase (air/ITO) (B) or the three-phase (air/ITO/glass) (C) Fresnel equations of reflection.

sample was calculated from the Fresnel equations for reflection at a single dielectric interface (two-phase model (air/ITO)) (B) or the three-phase (air/ITO/glass) (C) Fresnel equations of reflection using the Drude free-electron model to determine the dielectric function of the ITO. The calculated reflectance for both the two- and the three-phase Fresnel equations for reflection accurately models the observed trends in reflectance and the position of the plasma frequency with varying angles of incidence determined experimentally.

Figure 3A and B shows the experimental reflectance FTIR spectra in the region of the plasma frequency for ITO thin films of three different resistances (7−14 Ω/□) recorded at an incident angle of 60° with p-polarized radiation. Figure 3A also shows the calculated reflectance spectra obtained from the Drude free-electron model and the Fresnel equations for a single dielectric interface (two-phase, air/ITO), while the three-phase (air/ITO/glass) was used to obtain the calculated reflectance in Figure 3B. Figure 3A and B illustrates that the observed plasma frequency of ITO was a function of sheet resistance. A red shift in the observed plasma frequency was observed as the sheet resistance of the metal oxide electrode decreased. The fitted parameters for the Drude free-electron model for these ITO electrodes are listed in Table 1 using a constant value of 3.8

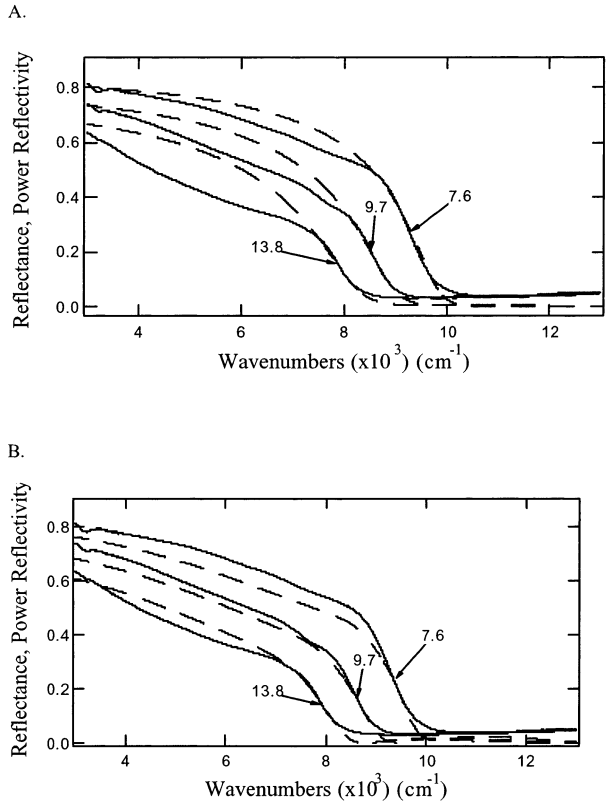

Figure 3. Experimental (solid) reflectance FTIR and calculated (dashed) power reflectivity spectra of three ITO electrodes with sheet resistances of 7.6, 9.7, and 13.8 Ω/□ for p-polarized radiation in the near-IR region using either the two-phase (air/ITO) (A) or the three-phase (air/ITO/glass) (B) Fresnel equations of reflection.

TABLE 1: The Electronic Scattering Time and Plasma Frequency of Three Different ITO Electrodes with Different Sheet Resistances As Determined from Fitting the Experimental Reflectance Data Using the Drude Free-Electron Model with a Constant Value of 3.8 for the High Frequency Dielectric Value To Determine the Dielectric Function of the ITO Thin Film and the Two-Phase (Air/ITO) (A) or the Three-Phase (Air/ITO/Glass) (B) Fresnel Equations for Reflection

sheet resistance (Ω/□)	electronic scattering time (τ) (10^{-15} s)	plasma frequency (ω_p) (cm^{-1})
	(A) Two Phase	
7.6	6.0	17 200
9.7	4.8	15 800
13.8	4.0	14 650
	(B) Three Phase	
7.6	7.0	17 100
9.7	5.6	15 900
13.8	4.8	14 900

for the high-frequency dielectric constant using the two- and three-phase Fresnel equations for reflection, respectively. The values in Table 1 show that both the plasma frequency and the electronic scattering time decreased as the sheet resistance of the ITO electrode increased. The value of the plasma frequency (ω_p) is dependent on the charge carrier density (n) and the effective electron mass (m) of the ITO thin film as defined by the Drude free-electron model defined in eq 2. The value of the plasma frequency affects the observed sharp decrease in reflectance, while the electronic scattering time affects the curvature of the reflectance spectrum near the observed plasma frequency. The two parameters of plasma frequency, the charge carrier density and effective electron mass, are coupled and cannot be individually determined in these experiments. The

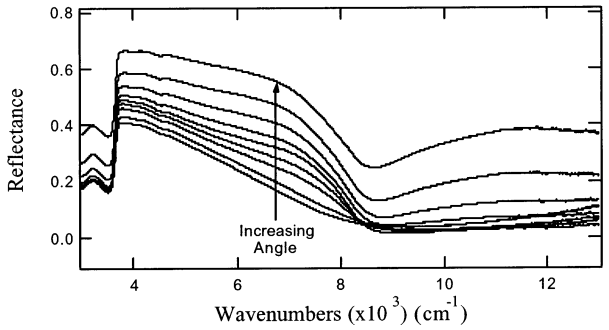

Figure 4. Experimental reflectance FTIR spectra of a thin film of ITO (13.8 Ω/□) on a glass substrate recorded in a air/glass/ITO sampling geometry for incident angles of 40−80° to the surface normal for p-polarized radiation in the near-IR region.

Drude free-electron model and the Fresnel equations of reflection accurately model the region of the reflectance spectra near the plasma frequency. However, the two-phase model calculates an overall higher absolute reflectance than that experimentally observed at wavenumbers lower in energy than the plasma frequency. The three-phase Fresnel equations of reflection more accurately fit the experimental reflectance of the different ITO samples in the entire near-IR region studied. Therefore, the shifts in the observed plasma frequency and curvature of the experimental reflectance spectra of ITO thin films with varying sheet resistances were successfully calculated using these theoretical models. The two- or three-phase Fresnel equations of reflection calculated plasma frequencies that differed by ∼100−250 cm^{-1}, while the electronic scattering times were ∼5−6 ($\times 10^{-16}$) s higher using the three-phase model as compared to the two-phase model.

The observed trends in the reflectance and plasma frequency on the sheet resistance of ITO thin films complement our earlier reflectance FTIR data in the mid-IR.[45] In this work, the following relationship between the plasma frequency (ω_p) and sheet resistance (R) was suggested (eq 11):[45]

$$\omega_p = \left(\frac{1}{Rt\epsilon_o\tau}\right)^{1/2} \tag{11}$$

where t is the thickness of the ITO film. However, only trends in the mid-IR reflectance suggestive of the onset of the plasma frequency were used to support this relationship. In the current work, the relationship between the plasma frequency and the sheet resistance and the electronic scattering time is confirmed. Figure 5A and B shows the linear dependence of the plasma frequency with the inverse square root of the sheet resistance (R) and electronic scattering time (τ), respectively, using the optical parameters from fitting the experimental reflectance FTIR data with the Drude free-electron model and the three-phase Fresnel equations of reflection (Table 1B).

Figure 4 shows the experimental variable angle reflectance FTIR spectra of a thin film of ITO (13.8 Ω/□) deposited on a glass substrate with p-polarized radiation impinging on the backside of the ITO thin film (air/glass/ITO sampling geometry) in the near-IR. This sampling geometry in contrast to air/ITO/glass sampling geometry used previously illustrates that the plasma frequency of ITO can also be monitored in an alternative geometry that would be beneficial when studying surface events (binding) on the ITO thin film from solution. This figure shows the angular dependence of the reflectance of the sample and the position of the observed plasma frequency for incident angles of 40−80° relative to the surface normal. The plasma frequency

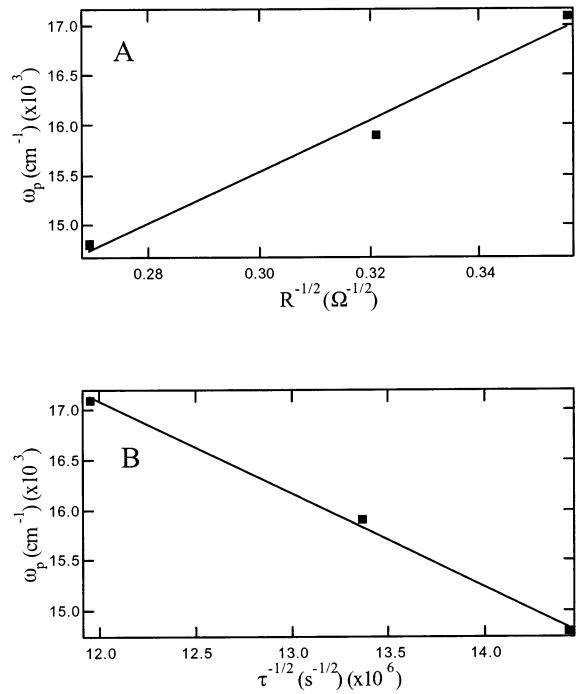

Figure 5. Plot of the plasma frequency (ω_p) dependence on the inverse square root of the sheet resistance (R) (A) and electronic scattering time (τ) (B) of ITO.

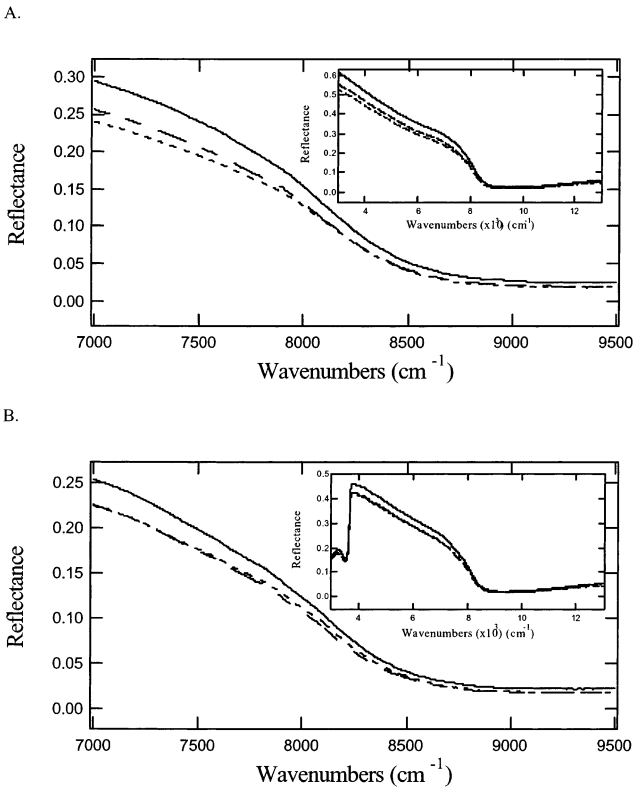

Figure 6. Experimental reflectance FTIR spectra of bare ITO (solid), an adlayer of 12-phosphonododecanoic acid on ITO (short dashed), and an adlayer of 1-hexadecanethiol on ITO (long dashed). The spectra were recorded at an incident angle of 60° with p-polarized radiation. The sampling geometry was either air/adlayer/ITO/glass (A) or air/glass/ITO/adlayer (B).

shifts to lower energy as the incident angle decreases, and the reflectance drops substantially at wavenumbers higher than the plasma frequency. However, the observed plasma frequency transition of the ITO is not as sharp in this sampling geometry (air/glass/ITO) as the air/ITO/glass geometry, and the observed reflectance is lower throughout the spectral region. The reflectance reaches a maximum at ~4000 cm^{-1}, where the glass substrate becomes nearly transparent to the radiation and stays transparent throughout the rest of the near-IR region of interest. Therefore, this sampling geometry (air/glass/ITO) is a second geometry that can be used in monitoring the optical properties (plasma frequency and reflectivity) of ITO.

Figure 6A and B illustrates the effect of a surface adlayer on the reflectivity and plasma frequency of ITO in the near-IR region at an incident angle of 60° with p-polarized radiation. The experimental reflectance FTIR spectra in Figure 6A were recorded in an air/adlayer/ITO/glass sampling geometry, while an air/glass/ITO/adlayer sampling geometry was used to measure the reflectance FTIR spectra in Figure 6B. An adlayer of 12-phosphonododecanoic acid or 1-hexadecanethiol on ITO[31] was used to illustrate the effect of adlayer formation on the optical properties of ITO. In both of the sampling geometries (Figure 6A and B), the reflectance and observed plasma frequency of ITO decrease due to the presence of either of these adlayers relative to bare ITO. Therefore, both the shift in the plasma frequency and the change in reflectivity in the near-IR of ITO due to adlayer formation can be utilized to observe binding events such as the formation of an adlayer on ITO.

Other metal oxide thin films such as fluorine-doped tin oxide (SFO) have optical properties similar to those of ITO in the near-IR. Figure 7A and B shows the observed reflectance FTIR spectra of a SFO deposited on a glass substrate recorded in the same two sampling geometries utilized with the ITO thin films with p-polarized light and incident angles ranging from 40 to 80° relative to the surface normal. Figure 7A and B was recorded in the air/SFO or air/glass/SFO sampling geometry, respectively. The overall reflectivity of this thin film and the plasma frequency were lower than those of the ITO thin films studied for both sampling geometries; however, the overall trends in the reflectance were similar to those observed for ITO thin films. For instance, the plasma frequency red shifts and the reflectance of SFO thin films decrease with decreasing angle near the plasma frequency, while the reflectance decreases substantially after the plasma frequency relative to the reflectance prior to the onset of the plasma frequency. This decrease in reflectance was partly due to the higher sheet resistance (55.6 Ω/□) of SFO than the ITO films studied, while the change in the observed plasma frequency is due to differences in the charge carrier density and effective electron mass of SFO as compared to ITO. The plasma frequency transition in Figure 7B is not as sharp as the ITO transition in the same backside sampling geometry. However, the plasma frequency can be detected and monitored in this geometry. Similar to ITO, Figure 7A and B demonstrates that two sampling geometries are possible for monitoring the plasma frequency and reflectivity (optical properties) of SFO thin films.

Conclusion

The plasma frequency of indium tin oxide (ITO) thin films was observed experimentally by variable angle reflectance FTIR spectroscopy and was found to decrease as the sheet resistance of the ITO thin films increased. The electronic scattering time and reflectance of these films also decreased with increasing sheet resistance. These results confirmed previous work[45] concerning the dependence of the reflectance and plasma frequency on the sheet resistance of the ITO thin films. The Drude free-electron model and the two- or three-phase Fresnel equations of reflection were used to fit the experimental data

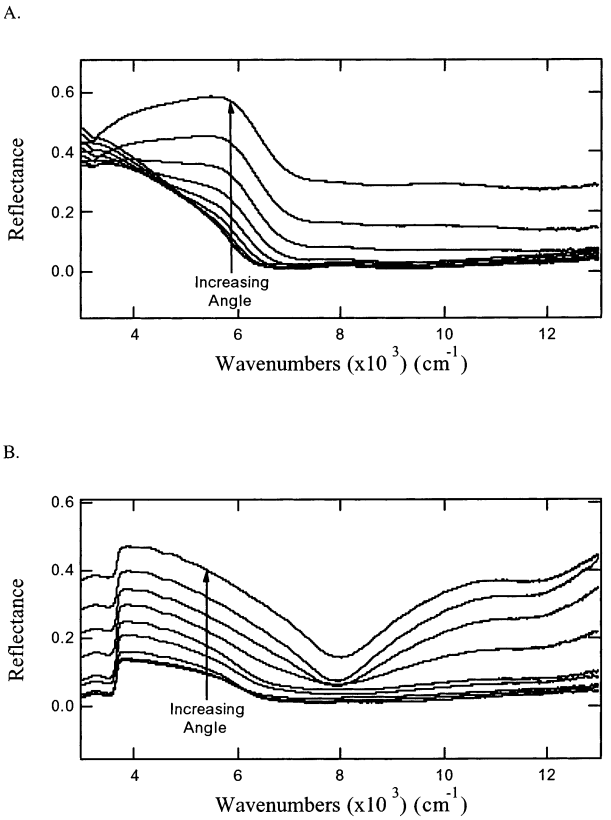

Figure 7. Experimental reflectance FTIR spectra for incident angles of 40−80° for SFO on a glass substrate with a sheet resistance of 55.6 Ω/□ recorded with p-polarized radiation in the near-IR region with either the air/SFO (A) or air/glass/SFO (B) sampling geometry.

to obtain values for the plasma frequency and electronic scattering time for the ITO thin films. These models accurately fit the area near the plasma frequency, but the two-phase model overestimated the absolute reflectance of the ITO thin films at lower wavenumbers than the plasma frequency, while the three-phase Fresnel equations of reflection fit the experimental data more closely throughout the entire near-IR region investigated. The calculated values of the plasma frequency and electronic scattering time differed by ∼100−250 cm^{-1} and 5−6 ($\times 10^{-16}$) s, respectively, between the two- and three-phase Fresnel equations of reflection. As expected from the Fresnel equations of reflection, the observed plasma frequency of ITO and reflectance just prior to the plasma frequency decreased with decreasing angles of incidence for p-polarized radiation. Surface adlayers of 12-phosphonododecanoic acid or 1-hexadecanethiol on the ITO thin films were shown to decrease the reflectivity and the observed plasma frequency of ITO using the air/adlayer/ITO/glass or air/glass/ITO/adlayer sampling geometries in the near-IR region. Fluorine-doped tin oxide (SFO) thin films were found to be less reflective and had a lower observed plasma frequency than the ITO thin films studied. The optical properties of these metal oxide thin films determined from reflectance FTIR spectroscopy offer a direct probe, specifically the plasma frequency and reflectivity, to monitor surface events such as adlayer formation (binding of molecules to the surface) or chemical modification of these metal oxide films. These properties could be monitored *in situ* to yield kinetic information on the binding of molecules to surface bound material or directly to these thin film metal oxide surfaces. The multiplex advantage of FTIR spectroscopy allows for the simultaneous determination of the reflectance over a broad spectral range at a fixed or variable angle of incidence instead of monitoring only the reflectance at a single wavelength, while incrementally varying the incident angle typically done with surface plasmon resonance (SPR) protocols using metal surfaces.[39] The sensitivity of ITO thin films is such that surface adlayer formation on ITO can easily be observed in the change in reflectivity and the plasma frequency of ITO, while the two different sampling geometries offer flexibility in monitoring the observed plasma frequency and reflectivity of these metal oxide thin films during surface modifications or annealing procedures.

Acknowledgment. S.H.B. was supported by the NIH Biotechnology Training Grant T32-GM08776.

Supporting Information Available: Experimental reflectance FTIR spectra of ITO deposited on a fused quartz substrate. This material is available free of charge via the Internet at http://pubs.acs.org.

References and Notes

(1) Tamada, M.; Koshikawa, H.; Hosoi, F.; Suwa, T. *Thin Solid Films* **1998**, *315*, 40−43.
(2) Purvis, K.; Lu, G.; Schwartz, J.; Bernasek, S. *J. Am. Chem. Soc.* **2000**, *122*, 1808−1809.
(3) VanderKam, S.; Gawalt, E.; Schwartz, J.; Bocarsly, A. *Langmuir* **1999**, *15*, 6598−6600.
(4) Oh, S.; Han, S. *Langmuir* **2000**, *16*, 6777−6779.
(5) Armistead, P.; Thorp, H. *Anal. Chem.* **2000**, *72*, 3764−3770.
(6) Armistead, P.; Thorp, H. *Anal. Chem.* **2001**, *73*, 558−564.
(7) Hamberg, I.; Granqvist, C. G. *J. Appl. Phys.* **1986**, *60*, R123−R159.
(8) Ambrosini, A.; Duarte, A.; Poeppelmeier, K. R.; Lane, M.; Kannewurf, C. R.; Mason, T. O. *J. Solid State Chem.* **2000**, *153*, 41−47.
(9) Kim, D.; Kim, S. *Thin Solid Films* **2002**, *408*, 218−222.
(10) Losurdo, M.; Barreca, D.; Capezzuto, P.; Bruno, G.; Tondello, E. *Surf. Coat. Technol.* **2002**, *151*−*152*, 2−8.
(11) Mryasov, O.; Freeman, A. *Phys. Rev. B* **2001**, *64*, 233111−233113.
(12) Hamberg, I.; Hjortsberg, A.; Granqvist, C. *Appl. Phys. Lett.* **1982**, *40*, 362−364.
(13) Hjortsberg, A.; Hamberg, I.; Granqvist, C. *Thin Solid Films* **1982**, *90*, 323−326.
(14) Bregman, J.; Shapira, Y.; Aharoni, H. *J. Appl. Phys.* **1990**, *67*, 3750−3753.
(15) Fan, J.; Bachner, F.; Foley, G. *Appl. Phys. Lett.* **1977**, *31*, 773−775.
(16) Shin, J.; Shin, S.; Park, J.; Kim, H. *J. Appl. Phys.* **2001**, *89*, 5199−5203.
(17) Bain, C.; Biebuyck, H.; Whitesides, G. *Langmuir* **1989**, *5*, 723−727.
(18) Karyakin, A.; Presnova, G.; Rubtsova, M.; Egorov, A. *Anal. Chem.* **2000**, *72*, 3805−3811.
(19) Kitano, H.; Taira, Y.; Yamamoto, H. *Anal. Chem.* **2000**, *72*, 2976−2980.
(20) Kittredge, K.; Fox, M.; Whitesell, J. *J. Phys. Chem. B* **2001**, ASAP article.
(21) Nakashima, N. *Langmuir* **1999**, *15*, 3823−3830.
(22) Naud, C.; Calas, P.; Commeyras, A. *Langmuir* **2001**, *17*, 4851−4857.
(23) Ringsdorf, H. *Macromolecules* **1997**, *30*, 5913−5919.
(24) Terril, R.; Tanzer, T.; Bohn, P. *Langmuir* **1998**, *14*, 845−854.
(25) Allara, D.; Nuzzo, R. *Langmuir* **1985**, *1*, 52−66.
(26) Allara, D.; Nuzzo, R. *Langmuir* **1985**, *1*, 45−52.
(27) Markovich, I.; Mandler, D. *J. Electroanal. Chem.* **2001**, *500*, 453−460.
(28) Oh, S.; Yun, Y.; Kim, D.; Han, S. *Langmuir* **1999**, *15*, 4690−4692.
(29) Yan, C.; Zharnikov, M.; Golzhauser, A.; Grunze, M. *Langmuir* **2000**, *16*, 6208−6215.
(30) Gardner, T.; Frisbie, C.; Wrighton, M. *J. Am. Chem. Soc.* **1995**, *117*, 6927−6933.
(31) Brewer, S.; Brown, D.; Franzen, S. *Langmuir* **2002**, *18*, 6857−6865.
(32) Synowicki, R. *Thin Solid Films* **1998**, *313*, 394−397.
(33) Gerfin, T.; Gratzel, M. *J. Appl. Phys.* **1996**, *79*, 1722−1729.
(34) Lee, D.; Vuong, K.; Sr., R. C.; Wang, X. W. *Mater. Lett.* **1996**, *28*, 179−182.
(35) Zotti, G.; Schiavon, G.; Zecchin, S.; Berlin, A.; Pagani, G. *Langmuir* **1998**, *14*, 1728−1733.

(36) Li, L.; Wang, R.; Fitzsimmons, M.; Li, D. *J. Phys. Chem. B* **2000**, *104*, 11195−11201.

(37) Fowles, G. *Introduction to Modern Optics*, 2nd ed.; Dover Publications: New York, 1989.

(38) Wooten, F. *Optical Properties of Solids*; Academic Press: San Diego, 1972.

(39) Brockman, J.; Nelson, B.; Corn, R. *Annu. Rev. Phys. Chem.* **2000**, *51*, 41−63.

(40) Stjerna, B.; Olsson, E.; Granqvist, C. *J. Appl. Phys.* **1994**, *76*, 3797−3817.

(41) Ray, S.; Karanjai, M.; Dasgupta, D. *Thin Solid Films* **1997**, *307*, 221−227.

(42) Mwamburi, M.; Wackelgard, E.; Roos, A. *Thin Solid Films* **2000**, *374*, 1−9.

(43) Philipp, H. In *Handbook of Optical Constants of Solids*; Palik, E., Ed.; Academic Press: San Diego, 1985; pp 749−763.

(44) Hansen, W. *J. Opt. Soc. Am.* **1968**, *58*, 380−390.

(45) Brewer, S. H.; Franzen, S. *J. Alloys Compd.* **2002**, *338*, 73−79.